Observed decadal changes in downward wave coupling between the stratosphere and troposphere in the Southern Hemisphere

Nili Harnik†, Judith Perlwitz††, and Tiffany A. Shaw†††

†*Deprtment of Geophysics and Planetary Sciences Tel-Aviv University, Tel Aviv, Israel*
††*Cooperative Institute for Research in Environmental Sciences, University of Colorado, Boulder, Colorado**
†††*Lamont-Doherty Earth Observatory and Department of Applied Physics and Applied Mathematics, Columbia University, New York, New York*

Contact:
Nili Harnik- harnik@tau.ac.il
Department of Geophysics
Tel Aviv University
Israel, 69978.

**Judith Perlwitz is also at NOAA/Earth System Research Laboratory, Physical Sciences Division, Boulder, Colorado*

Submitted to the Journal of Climate

October 6, 2010

Abstract

Downward wave coupling dominates the intraseasonal dynamical coupling between the stratosphere and troposphere in the Southern Hemisphere. The coupling occurs during late winter and spring when the stratospheric basic state forms a well-defined meridional waveguide, which is bounded above by a reflecting surface. This basic state configuration is favorable for planetary wave reflection and guides the reflected waves back down to the troposphere where they impact wave structures. In this study we analyze decadal changes in downward wave coupling using the Modern Era Retrospective-analysis for Research and Application (MERRA) data set.

A cross-spectral correlation analysis applied to geopotential height fields and a wave geometry diagnostic, applied to zonal-mean zonal wind and temperature data, are used to understand decadal changes in planetary wave propagation. It is found that downward wave-1 coupling from September to December has increased over the last three decades owing to significant increases at the beginning and end of this four-month period. The increased downward wave coupling is caused both by an earlier onset of the vertically bounded meridional waveguide configuration and a persistence of this configuration into December. The latter is associated with the observed delay in vortex breakup. The results point to an additional dynamical mechanism whereby the stratosphere has influenced tropospheric climate in the Southern Hemisphere.

1 Introduction

During the last three decades the extratropical Southern Hemisphere has undergone significant climate changes. These changes are most apparent during spring and early summer and include a cooling of the polar stratosphere, a delay of the breakup of the polar vortex and an increase in the strength of the tropospheric westerlies together with surface cooling over the Antarctic interior and a warming over the Antarctic peninsula (e.g. Waugh et al., 1999; Thompson and Solomon, 2002). These changes have been mostly attributed to stratospheric polar ozone depletion (e.g. Gillett and Thompson, 2003), which affects the troposphere via annular mode dynamics (see Son et al., 2010, for an overview of possible mechanisms). More recently, it has been noted that there is a strong non-zonal component to Southern Hemisphere climate trends (e.g. Johanson and Fu, 2007), which are associated with significant changes in planetary wave structure from the troposphere to the stratosphere (Neff et al., 2008; Lin et al., 2009; Hu and Fu, 2009). Hu and Fu (2009) attributed the stratospheric changes in planetary wave structure to an increase in upward planetary wave activity flux caused by changes in sea surface temperature (SST), however the nature of decadal changes in wave dynamics are still not well understood.

It is well known that wave activity propagation from the troposphere to the stratosphere in the Southern Hemisphere maximizes during austral spring (Randel, 1988). When the upward propagating waves reach the stratosphere they either dissipate and initiate zonal-mean stratosphere-troposphere coupling or they are reflected downward towards the troposphere, which results in downward wave coupling (Perlwitz and Harnik, 2004; Harnik, 2009). Recently, Shaw et al. (2010a) showed that climatological downward wave coupling is stronger than zonal-mean coupling on the intraseasonal time scale in the Southern Hemisphere, particularly during austral spring. They found significant downward wave coupling beginning in September-October, peaking in October-November, and decaying towards the breakup of the vortex in November-

December. The strong wave coupling was attributed to the formation of a bounded wave geometry involving a high-latitude meridional wave guide in the lower stratosphere, bounded above by a vertical reflecting surface, which occurs as part of the seasonal cycle. The meridional wave guide focuses the upward propagating waves toward the vertical reflecting surface in the stratosphere, and upon reflection, back down into the troposphere.

The goal of this paper is to investigate the impact of the observed changes in the extratropical Southern Hemisphere on downward wave coupling between the stratosphere and troposphere. We show that downward wave coupling from September to December has increased significantly over the last three decades due to changes in the wave geometry. The data sets and the analysis approach are described in Sec. 2, the results presented in Sec. 3, and the findings are summarized in Sec. 4.

2 Data and analysis approach

The reanalysis data used in this study are the daily three-dimensional geopotential heights, and zonal-mean zonal wind and temperature fields from the Modern Era Retrospective-analysis for Research and Application (MERRA) reanalysis data set (Rienecker et al., 2008; Schubert et al., 2008) covering the period from 1979 to 2009. Shaw et al. (2010a) used the ECMWF 40-year Re-Analysis (ERA-40) data set in their study. They noted that the ERA-40 and MERRA reanalyses were consistent in their climatologies of downward wave coupling in the Southern Hemisphere.

Downward wave coupling is analyzed using the diagnostics of Shaw et al. (2010a). A cross-spectral correlation technique (Randel, 1987) is used to isolate upward and downward propagating planetary wave signals. The diagnostic considers two geopotential height Fourier coefficients of wavenumber k at two different latitudes and heights and determines their coherence correlation and phase as a function of time lag. Statistically significant cross correlations for time

lags when the stratosphere leads the troposphere indicate downward wave coupling. We focus on zonal wave-1 and use a reference latitude band from 45 to 80°S and a reference level at 500 hPa. Further details can be found in Shaw et al. (2010a). To examine decadal variations, we apply the diagnostic to 10-year periods. To examine seasonal variations, we use a few reference time series, spanning the following four time periods: September 1 - December 16, September 1 - October 16, October 1 - November 15, November 1 - December 16. Considering the autorcorrelation of tropospheric and stratospheric wave-1 fields, decadal stratospheric correlation coefficients greater than 0.18 and 0.2 are significant at the 99% level for the four-month and two-month correlations, respectively.

The wave geometry diagnostic of Harnik and Lindzen (2001) is used to relate the downward wave coupling to the basic state (i.e. to the zonal-mean zonal wind and temperature). The diagnostic separates the more commonly used index of refraction into vertical and meridional wave number contributions. As for the squared index of refraction, waves propagate in the vertical direction when $m^2 > 0$, are evanescent when $m^2 < 0$, and are reflected when they reach a surface where $m^2 = 0$. Similarly, wave propagation in the meridional direction depends on the sign of l^2. The wave geometry diagnostic is used to determine whether the basic state allows wave propagation in the vertical and meridional directions. The wavenumber results presented here are based on 5-day running means of zonal-mean zonal wind and temperature data. The MERRA data were sub-sampled at every second latitude (2.5 degree resolution) to facilitate handling of the data. The results were very similar to those when the full (1.25 degree resolution) data was used. The wavenumbers were averaged using their squared values as follows: $\langle m \rangle = \sqrt{|\langle m^2 \rangle|} \times sign(\langle m^2 \rangle)$ where $\langle \cdot \rangle$ denotes an average and $|\cdot|$ denotes the absolute value. Further details can be found in Shaw et al. (2010a) and Harnik and Lindzen (2001).

3 Results

We begin by examining the cross-correlations during the three decades [1979-1988], [1989-1998], [1999-2001,2003-2009] (the anomalous stratospheric sudden warming year 2002 is excluded from the last decade). Fig. 1 shows the wave-1 cross-correlations with a reference latitude band from 45 to 80°S at 500 hPa, for vertical levels from 500 to 1 hPa and for time lags between -10 and 10 days, for the September-December, September-October, October-November, and November-December periods mentioned in Sec. 2 (top to bottom rows, respectively). Only significant correlation values are contoured. The shading in the second and third decades indicates regions where the difference in correlations relative to the first decade are significant at the 90%, 95%, and 99% levels. Statistical significance is quantified using a Monte-Carlo test, by first selecting two random 10-year sub-sets of the full 31-year data set, then calculating the time-lagged correlation for each subset, and finally, subtracting the two to obtain the difference in correlation as a function of time-lag and height. This process is repeated 500 times, for each of the sub-seasonal reference periods, to determine the significance levels.

Following Shaw et al. (2010a) we begin by considering the entire reflective season (September to December). All decades show significant upward propagation (significant correlations for positive lags) and significant downward propagation (significant correlations for negative lags). The latter indicates downward wave coupling. The shadings indicate that the correlations for negative lags increased significantly during the second and third decades, implying that downward wave coupling has increased with time over the past thirty years. The significant increases occur at lags of -3 days for the stratosphere (shading between $20-1$ hPa top row, middle and right columns), and around -7 days for the troposphere (shading between $500-200$ hPa top row, middle and right columns). This is consistent with downward reflection of waves which originate in the troposphere. There is also an increase in the 500 hPa $+7$ day correlations

during the second decade (top row middle column). This symmetric change in the reference height correlations (at ± 7 days) is also consistent with the tropospheric waves propagating to the stratosphere and reflecting back down. It is important to note that the changes in the tropospheric correlations may also indicate a change in the wave source.

The two-month correlations show that during 1979-1988 downward correlations were only significant during October-November, where as during the later two decades the correlations became significant during September-October and lasted into November-December as well. The shadings indicate significant increases in downward correlations during September-October (second row) and November-December (last row) but not during October-November (third row). This suggests the increase in downward correlations during September-December mostly occurred at the beginning and end of the reflective season, but not during its peak. For the November-December period, we also see significant increases in the stratospheric positive time lag correlations, which are suggestive of increased upward propagation. We will show later on that this is consistent with a tendency of the vortex to last longer during the later two decades. During the second decade the September-October correlations (middle column, second row) increased significantly also in the troposphere, for both negative and positive time lags, suggesting changes both in the internal tropospheric wave dynamics (i.e. the wave sources) and in downward reflection from the stratosphere.

Next we examine the decadal changes in the basic state using the wave geometry diagnostic. As mentioned previously, the wave geometry assesses the wave propagation characteristics of the basic state. The ability of waves to propagate in the vertical and meridional direction is determined by looking at the vertical (m) and meridional (l) wavenumbers separately. Fig. 2 shows decadal averages of the mean vertical wavenumber for September 1st to October 16th. The shading indicates regions where waves cannot propagate in the vertical direction (wave

evanescence regions), and the evanescent region boundary (thick black contours), is called a reflecting surface. In particular the reflecting surface in the upper stratosphere high latitudes will reflect upward propagating waves back downwards. The decadal panels suggest that the reflecting surface moved down and widened over the last three decades with relatively little change in the vertical wavenumber at lower levels. Fig. 2d shows the yearly time series of the squared vertical wavenumber averaged from 50-70°S and 5-1 hPa (representing the vertical boundary of the wave guide). Time series of the squared wavenumbers are used to represent the transition between periods of wave propagation (real m, l and $m^2 > 0$, $l^2 > 0$), to wave evanescence (imaginary m, l and $m^2 < 0$, $l^2 < 0$). Consistent with the decadal panels, there is a clear negative trend (significant at the 99% level, based on a single-sided t-test, with $|t| = 2.35$) suggesting that the upper stratosphere between 50-70°S has became more evanescent for vertical wave propagation over the last three decades.

Shaw et al. (2010a) examined the climatological seasonal evolution of the vertical reflecting surface, and found that it forms in September at around 1 hPa, and descends to below 10 hPa during October. Examining the mean daily seasonal evolution during each of the three decades (not shown) suggests this seasonal descent occurs earlier in the second and third decade, compared to the first. While in the earliest decade, the September 1- October 16 mean vertical wavenumber is comprised mostly of days when the reflecting surface is high (Fig. 2a), in the later decades it includes more days with a low vertical reflecting surface (Fig. 2b-c).

Shaw et al. (2010a) showed that the formation of a vertical reflecting surface is not sufficient for downward wave coupling because the waves can disperse in the meridional direction. Downward wave couping occurs when there is a high-latitude meridional waveguide, which is bounded above by a reflecting surface. Fig. 3 shows the meridional wavenumbers for the same periods of Fig. 2. The shading now indicates regions where the waves cannot propagate in

the meridional direction. For all decades, we see a clear meridional waveguide (the unshaded contoured meridional propagation region between 40-60°S, which is bounded by the shaded regions). In order to visualize the meridional-vertical wave propagation geometry, we also plotted the vertical reflecting surface (solid thick line). We see that during the last two decades, the lower stratospheric meridional waveguide is narrower (the evanescent region at 40°S, 100-30 hPa appears in the first decade and widens with time), and the vertical reflecting surface is lower so that it better covers the region where the waves propagate upwards. Shaw et al. (2010a) called this wave geometry configuration, in which the reflecting surface spans the meridional waveguide, *a bounded wave geometry*. Waves propagating vertically along the meridional waveguide region are reflected down, and guided back to the troposphere where they influence the planetary wave field. Shaw et al. (2010a) also showed that the climatological meridional waveguide is much narrower during late winter and spring than it is during early winter. We find that the transition to a narrower waveguide occurs earlier in the second two decades compared to the first (not shown). The yearly time series of the squared meridional wavenumber averaged from 100-30 hPa and 36-46°S (representing the equatorward boundary of the wave guide, Fig. 3d) shows a clear negative trend, which is significant at the 97% level based on a single-sided t-test ($|t| = 2.01$). The combined changes in vertical and meridional wavenumbers are consistent with the increase in the September-October downward wave cross-correlations shown in Fig. 1. While the bounded wave geometry which is favorable for downward wave coupling starts in September during the 1970s, it starts in early October during the 1980s and 1990s.

Harnik and Lindzen (2001) found that wave reflection in the Southern Hemisphere occurred during winter when the vertical shear of the zonal mean wind (U_z) became negative in the upper stratosphere. This negative shear forms in mid-winter as part of the climatological seasonal cycle. Fig. 4 shows that U_z averaged from 50-70°S and 5-1 hPa has decreased significantly with

time (note that we removed the sudden warming year 2002 to calculate the trend), however it is not strongly correlated with the averaged vertical wavenumber in Fig. 3d. This suggests that the increase in wave reflection, and hence downward wave coupling, is partly due to a stronger upper stratospheric negative wind shear in high latitudes.

Previous studies have shown that the breakup of the polar vortex has been delayed in recent decades (e.g. Neff, 1999; Waugh et al., 1999). This has been attributed to ozone depletion (e.g. Haigh and Roscoe, 2009). We expect this delay in vortex breakup to allow upward wave propagation and downward wave reflection to last longer into December and can therefore be used to explain the observed increase in upward and downward wave coupling during November-December (bottom row of Fig. 1). To identify vortex breakup we calculate the mid-stratospheric (30-10 hPa) zonal-mean zonal wind - $\langle U(30-10)\rangle$ and define the vortex breakup date as the day on which the $55-75°$S mean $\langle U(30-10)\rangle$ first becomes negative during November-December. The vortex breakup day, counted from January 1st, is denoted by *df* and plotted in Fig. 5. There is a lot of variability in the vortex breakup date, however there is a discernible positive trend[1]. The largest and most significant trend occurs from 1979 to 1999 (thick straight line) and is statistically significant at the 98.8% level based on a 1-sided t-test ($|t| = 2.42$), while the trend over the entire period (thin straight line) is only significant at the 88% level ($|t| = 1.16$). If the sudden warming year 2002 is removed, the trend over the entire period is significant at the 97.1% level ($|t| = 1.97$). The smaller trend significance for the longer period is consistent with the saturation of ozone depletion observed since the late 1990 (Langematz and Kunze, 2006). However, the leveling-off of the trend may also be associated with increased wave activity, which would lead to an earlier breakup date (e.g. Hu and Fu, 2009; Akiyoshi et al., 2009).

[1]The nature of both interannual variability and trend of the vortex break up are consistent with the timing of the initial spring increases in the stability in the layer from 150-100 hPa determined based on rawinsonde data for the period from 1979 to 1998 Neff (1999) and its update to 2009 (Bill Neff, personal communications))

To understand the effect of the delay in vortex breakup date on the wave geometry we calculate, for each year, the vertical and meridional wavenumbers during 20 day periods before and after vortex breakup (i.e. $m(df-25:df-5)$, $l(df+5:df+25)$, with the averaging period kept within the same calendar year) and then average over all years. Figs. 6a,b show the pre- and post- vortex breakup wave geometries. Before vortex breakup, vertical wave propagation can occur up to about 10hPa and there is a well defined high-latitude meridional waveguide in the lower stratosphere (between 100-30hPa). This is a characteristic spring wave geometry. After vortex breakup, the wave geometry is more characteristic of a summer stratospheric basic state, with vertical wave propagation inhibited above 100hPa and the subtropical tropospheric waveguide tilting poleward in the lower stratosphere. To asses trends we calculate yearly time series of m and l from October 31-December 20 (chosen to include all vortex breakup dates: $min(df)-5:max(df)+5$). Fig. 6c,d show the yearly time series of m^2 averaged between 55-15 hPa and 50-70°S and l^2 averaged between 100-10 hPa and 40-50°S. There are clear correlations between the averaged squared wavenumbers and the vortex breakup date time series. The correlations between the detrended df and the detrended $\langle m^2 \rangle$ and $\langle l^2 \rangle$ are 0.79 and -0.83, respectively. The 1979-2009 and 1979-1999 trends are shown (thin and thick straight lines, respectively) with the corresponding $|t|$ values stated on the plot in regular and bold face, respectively. As for df, the linear trends in m^2 and l^2 are significant at least at the 99% level during the first two decades and there is a saturation in the third decade. Removing the year 2002 increases the significance of the 1979-2009 trend, especially for l^2 ($|t|$ values of 1.69 instead of 1.16 for df, 2.58 instead of 1.83 for m^2 and 2.77 instead of 2.00 for l^2). The results clearly demonstrate that the delay in vortex breakup date causes the bounded wave geometry to last longer leading to enhanced downward wave reflection and hence larger downward wave coupling during November-December.

Fig. 1 showed that the September-October and November-December correlations increased significantly with time whereas the October-November correlations did not show significant trends. Consistently, we find that the wave geometry did not change significantly from October 17 to the vortex breakup date *df* (not shown). Thus, the main changes in downward wave coupling result from changes at the beginning and end of the wave reflective season. The combination of the earlier onset of the bounded wave geometry (from early October to September) and vortex breakup shifting from late November to December causes the significant increase in the September to December downward wave coupling.

4 Summary and discussion

This paper examines decadal changes in downward wave coupling using the MERRA reanalysis data set from 1979 to 2009. Downward wave coupling is identified using cross-coherence correlations between stratospheric and tropospheric wave-1 geopotential height fields. The wave coupling is related to the basic state using wave geometry diagnostics for stationary zonal wave-1. We find a significant increase in downward wave coupling during the September to December period, as well as during the September-October and November-December periods over the last three decades. The increase is related to a change in the timing of the bounded wave geometry configuration, which is favorable for downward wave coupling. The bounded wave geometry starts earlier in the season (early September) and lasts longer (into December) with little change in the middle of the reflective period (from mid-October to vortex breakup date).

The causes of the observed decadal changes in the wave geometry, which result in changes in the downward wave coupling, have not been attributed so far and are only partially understood. Our analysis reveals that the extension of the bounded wave geometry into November-December is most likely caused by a delay in the vortex breakup which has been linked to stratospheric

ozone depletion (Haigh and Roscoe, 2009). However increases in planetary wave driving during winter and early spring, which have been observed in the 2000s, also affect the vortex persistence (Langematz and Kunze, 2006). The changes in the wave geometry during September-October are clearly related to changes in the stratospheric vortex structure, particularly in the upper stratosphere in mid and high latitudes, however the contribution of stratospheric ozone changes, SST changes and other processes to these mean flow changes are not clear.

Because the trend calculations are based on a reanalysis product we cannot preclude impacts of the changing observing system on the decadal changes, especially in the mid to upper stratosphere. We also note that the meridional and vertical wavenumber calculations involve highly derived quantities which increases the uncertainties in their trend estimates. However, we found that the MERRA decadal changes in both the wave geometry and wave-1 cross correlations for the period 1979 to 1998 were very close to those from the ERA-40 reanalysis. Furthermore, the MERRA decadal cross-correlation changes during the period 1979 to 2009 agree well with similar estimates based on the National Centers for Environmental Prediction(NCEP)/Department of Energy (DOE) Atmospheric Model Inter-comparison Project (AMIP-II) reanalysis R2 Kanamitsu et al. (2002). Overall, the wave-1 decadal cross correlations are more reliable because they are directly based on geopotential heights, which is a class A reanalysis field in the troposphere and lower stratosphere[2]. The consistency of the two diagnostics (cross correlations and wave geometry) suggests that the changes in the wave geometry are also reliable and furthermore that the decadal changes in downward coupling are not an artifact of the changing observing system.

Atmospheric general circulation models can be used to assess the causes for the observed increase in downward wave coupling. However, the model must have a proper representation of the climatology of the stratospheric basic state and downward wave coupling (Shaw et al., 2010a).

[2]According to Kalnay et al. (1996), a reanalysis gridded field is classified as class A analysis variable when it is strongly influenced by observed data and hence most reliable.

In a companion paper, we use the Goddard Earth Observing System chemistry-climate model and attribute the increase of downward wave coupling in the model to ozone depletion (Shaw et al., 2010b). As in observations, the model shows an increase in downward cross correlations when forced with observed changes in halogens. These are related to ozone-induced changes in the wave geometry, which cause a delay in the vortex breakup date. When the model was run without ozone depletion there was no significant change in the downward wave coupling.

Previous studies have emphasized the importance of changes in zonal-mean stratosphere-troposphere coupling since 1979 and their impact on the Southern Hemisphere annular mode (see Son et al., 2010, for overview of identified mechanisms). More recently, studies have pointed out significant observed non-zonal decadal trends (Neff et al., 2008; Lin et al., 2009; Hu and Fu, 2009). Our study shows that in addition to changes in zonal-mean coupling there has been a significant change in downward wave coupling since 1979. Understanding to what degree changes in downward wave coupling explain the observed non-zonal decadal trends in the Southern Hemisphere is work in progress.

Acknowledgments

NH was supported by grant 1370/08 from the Israeli Science Foundation. JP acknowledges support from NASA Modeling and Analysis program. TAS was supported by a Post Doctoral Fellowship from the Natural Sciences and Engineering Research Council of Canada. The authors thank Bill Neff and Steven Pawson for their input and helpful discussions.

References

Akiyoshi, H. et al., 2009: A CCM simulation of the breakup of the antarctic polar vortex in the years 1980-2004 under the ccmval scenarios, *J. Geophys. Res.*, **114**, D03103, doi:10.1029/2007JD009261.

Gillett, N. P. and D. W. J. Thompson, 2003: Simulation of recent southern hemisphere climate change, *Science*, **302**, 273–275.

Haigh, J. D. and H. K. Roscoe, 2009: The final warming date of the antarctic polar vortex and influences on its interannual variability, *J. Clim.*, **22**, 5809–5819.

Harnik, N., 2009: Observed stratospheric downward reflection and its relation to upward pulses of wave activity., *J. Geophys. Res.*, **114**, D08120, doi:10.1029/2008JD010493.

Harnik, N. and R. S. Lindzen, 2001: The effect of reflecting surfaces on the vertical structure and variability of stratospheric planetary waves, *J. Atmos. Sci.*, **58**, 2872–2894.

Hu, Y. and Q. Fu, 2009: Stratospheric warming in Southern Hemisphere high latitudes since 1979, *Atmos. Chem. Phys.*, **9**, 4329–4340.

Johanson, C. M. and Q. Fu, 2007: Antarctic atmospheric temperature trend patterns from satellite observations., *Geophys. Res. Lett.*, doi:10.1029/2006GL029108.

Kalnay, E. et al., 1996: The NCEP/NCAR 40-year reanalysis project, *B. Am. Meteorol. Soc.*, **77**(434-471).

Kanamitsu, M., W. Ebisuzaki, J. Woollen, S.-K. Yang, J. J. Hnilo, M. Fiorino, and G. L. Potter, 2002: NCEP-DOE AMIP-II Reanalysis (R-2), *B. Am. Meteorol. Soc.*, **83**, 1631–1643.

Langematz, U. and M. Kunze, 2006: An update on dynamical changes in the arctic and antarctic stratospheric polar vortices, *Clim. Dyn.*, **27**, 647–660, doi:10.1007/s00382-006-0156-2.

Lin, P., Q. Fu, S. Solomon, and J. W. Wallace, 2009: Temperature trend patterns in Southern Hemisphere high latitudes: novel indicators of stratospheric change, *J. Clim.*, **22**, 6325–6341.

Neff, W., 1999: Decadal time scale trends and variability in the tropospheric circulation over the South Pole, *J. Geophys. Res.*, **104**, 27217–27251.

Neff, W., J. Perlwitz, and M. Hoerling, 2008: Observational evidence for asymmetric changes in tropospheric heights over Antarctica on decadal time scales, *Geophys. Res. Lett.*, **35**.

Perlwitz, J. and N. Harnik, 2004: Downward coupling between the stratosphere and troposphere: The relative roles of wave and zonal mean processes, *J. Clim.*, **17**, 4902–4909.

Randel, W. J., 1987: Study of planetary waves in the southern winter troposphere and stratosphere. Part 1: Wave structure and vertical propagation, *J. Atmos. Sci.*, **44**, 917–935.

Randel, W. J., 1988: The seasonal evolution of planetary-waves in the southern-hemisphere stratosphere and troposphere, *Q. J. R. Meteorol. Soc.*, **114**(484), 1385–1409.

Rienecker, M. M. et al., 2008: The GEOS-5 data assimilation system - documentation of versions 5.0.1, 5.1.0, and 5.2.0, *Technical Report Series on Global Modeling and Data Assimilation*, **27**, http://gmao.gsfc.nasa.gov/pubs/docs/Rienecker369.pdf.

Schubert, S. et al., 2008: *Assimilating Earth System Observations at NASA: MERRA and Beyond*, Third WCRP International Conference on Reanalysis, Tokyo, Japan, http://wcrp.ipsl.jussieu.fr/Workshops/Reanalysis2008/Documents/V1-104_ea.pdf.

Shaw, T. A., J. Perlwitz, and N. Harnik, 2010a: Downward wave coupling between the stratosphere and troposphere: the importance of meridional wave guiding and comparison with zonal-mean coupling, *J. Clim.*, in press.

Shaw, T. A., J. Perlwitz, and N. Harnik, 2010b: The impact of stratospheric ozone changes on downward wave coupling in the southern hemisphere, *J. Clim.*, submitted.

Son, S.-W. et al., 2010: The impact of stratospheric ozone on southern hemisphere circulation change: A multimodel assessment, In press.

Thompson, D. W. J. and S. Solomon, 2002: Interpretation of recent southern hemisphere climate

change, *Science*, **296**, 895–899.

Waugh, D., W. Randel, S. Pawson, P. Newman, and E. Nash, 1999: Persistence of the lower stratospheric polar vortices, *J. Geophys. Res.*, **104**, 27191–27201.

Figure Captions

Fig. 1. Correlation coherence for wave-1 averaged from 45 to 80°S at 500 hPa with vertical levels between 500 and 1 hPa during September to December (top row), September-October (second row), October-November (third row), and November-December (bottom row), for three decades: 1979-88 (left column), 1989-98 (middle column), and 1999-2009 (right column) excluding the sudden warming year of 2002. Since the correlations are relative to the $500hPa$ level, negative lags mean the stratosphere leads. Light, intermediate and dark shadings indicates regions in which the differences in correlation from the first decade are significant at the 90%, 95%, and 99% levels, respectively.

Fig. 2. Decadal mean vertical wavenumbers for September 1st-October 16th, for a) 1979-88, b) 1989-99, c) 1999-2009, excluding 2002. Evanescent regions (negative m^2) are shaded. Contour values, in units of $10^{-5}m^{-1}$, are 0 (thick), 4 (dashed), and $8, 10, 12, 16, 20$ (solid). d) Yearly values, and linear best fit regression (straight line) of the September 1-October 16 mean vertical wavenumber squared, averaged over $5-1hPa$, $50-70^oS$ (units of $10^{-9}m^{-2}$).

Fig. 3. Decadal meridional wavenumbers for September 1st-October 16th, for a) 1979-88, b) 1989-99, c) 1999-2009, excluding 2002. Evanescent regions (negative l^2) are shaded. Contour values, in units of rad^{-1}, are 2 (dashed), and $3, 4, 6$ (solid). Also shown is the vertical reflecting surface (thick solid lines) from Fig. 2. d) Yearly values, and linear best fit regression (straight lines) of the September 1-October 16 mean d) meridional wavenumber squared, averaged over $100-30hPa$, $36-46^oS$ (units of rad^{-2}).

Fig. 4. Yearly values of the September 1-October 16 mean vertical shear of the zonal mean wind, averaged over $5-1hPa$, $50-70^oS$ ($msec^{-1}/km$), along with the linear best fit regression. The sudden warming year 2002 is removed from the trend calculation.

Fig. 5. Yearly time series (circled line) with the linear trends and $|t|$ values based on 1979-2009 and 1979-1999 (thin and thick straight lines respectively) of the day on which the zonal mean wind, averaged over $30-10hPa$ $54-75^oS$, first becomes zero, counting from January 1 (excluding the September 2002 sudden warming).

Fig. 6. The 1979-2009 mean vertical and meridional wavenumbers for the 20 days before (a) and after (b) the final warming date, defined by the index of Fig. 5. The contouring and shading in plots a-b are the same as in Fig 3a-c. (c-d) Yearly time series (circled line) with the linear trends based on 1979-2009 and 1979-1999 (thin and thick straight lines respectively) of the October 31-December 20 mean c) vertical wavenumber squared averaged over $55-15hPa$, $50-70^oS$ (units of $10^{-8}m^{-2}$) and d) meridional wavenumbers squared, averaged over $100-10hPa$, $40-50^oS$ (units of rad^{-2}).

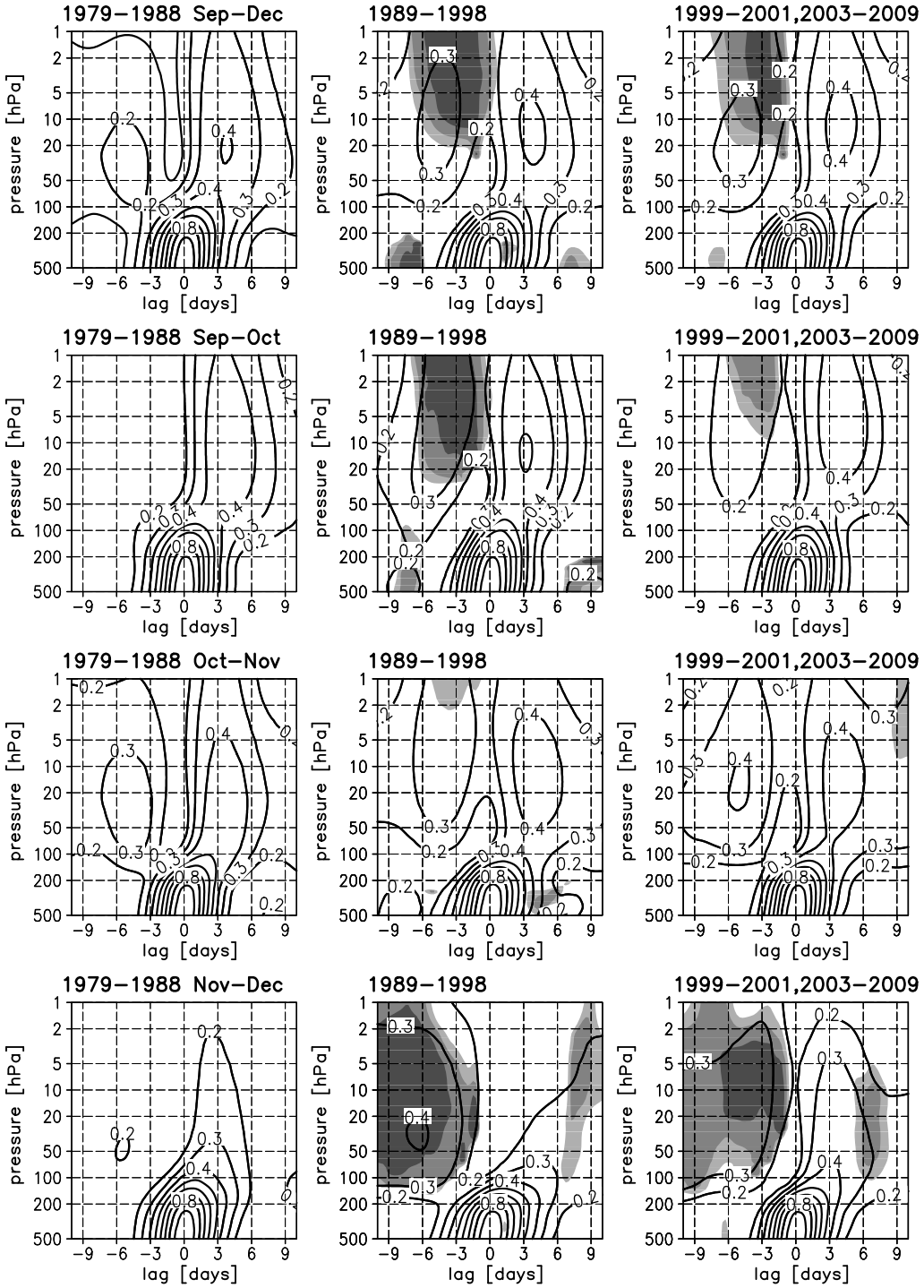

Figure 1: Correlation coherence for wave-1 averaged from 45 to 80°S at 500 hPa with vertical levels between 500 and 1 hPa during September to December (top row), September-October (second row), October-November (third row), and November-December (bottom row), for three decades: 1979-88 (left column), 1989-98 (middle column), and 1999-2009 (right column) excluding the sudden warming year of 2002. Since the correlations are relative to the $500hPa$ level, negative lags mean the stratosphere leads. Light, intermediate and dark shadings indicates regions in which the differences in correlation from the first decade are significant at the 90%, 95%, and 99% levels, respectively.

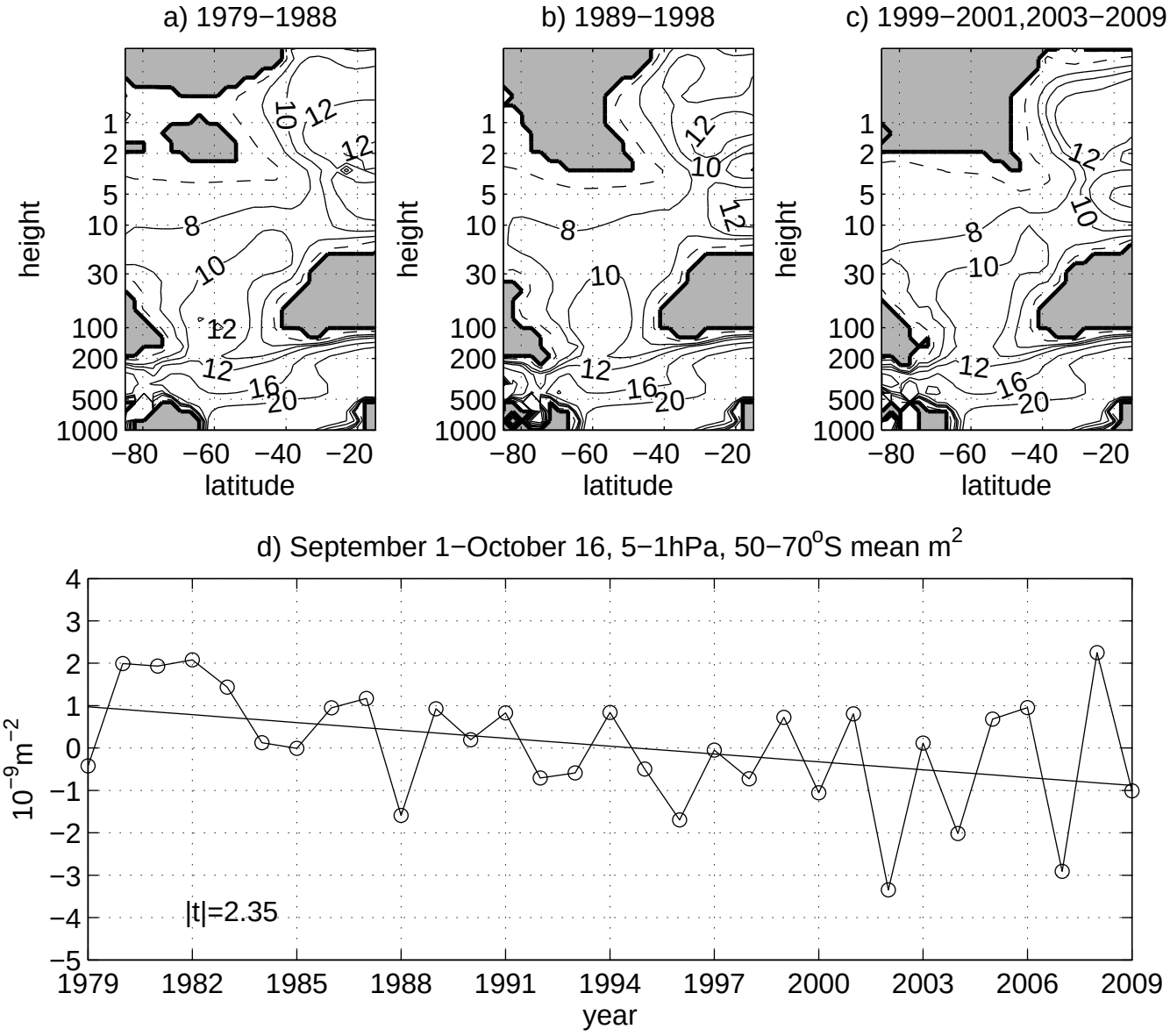

Figure 2: Decadal mean vertical wavenumbers for September 1st-October 16th, for a) 1979-88, b) 1989-99, c) 1999-2009, excluding 2002. Evanescent regions (negative m^2) are shaded. Contour values, in units of $10^{-5}m^{-1}$, are 0 (thick), 4 (dashed), and $8, 10, 12, 16, 20$ (solid). d) Yearly values, and linear best fit regression (straight line) of the September 1-October 16 mean vertical wavenumber squared, averaged over $5 - 1hPa$, $50 - 70^oS$ (units of $10^{-9}m^{-2}$).

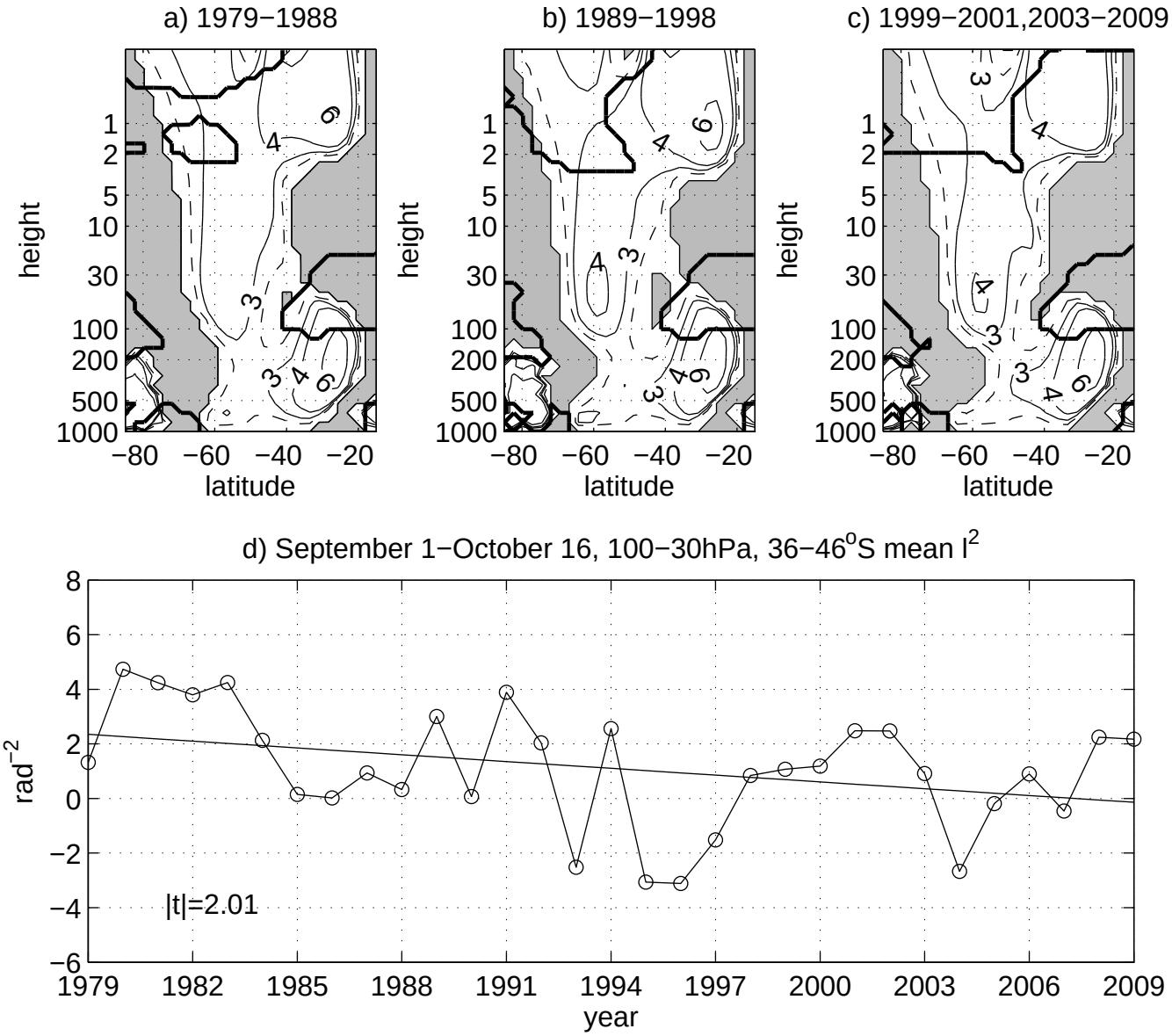

Figure 3: Decadal meridional wavenumbers for September 1st-October 16th, for a) 1979-88, b) 1989-99, c) 1999-2009, excluding 2002. Evanescent regions (negative l^2) are shaded. Contour values, in units of rad^{-1}, are 2 (dashed), and $3, 4, 6$ (solid). Also shown is the vertical reflecting surface (thick solid lines) from Fig. 2. d) Yearly values, and linear best fit regression (straight line) of the September 1-October 16 mean meridional wavenumber squared, averaged over $100-30hPa$, $36-46^oS$ (units of rad^{-2}).

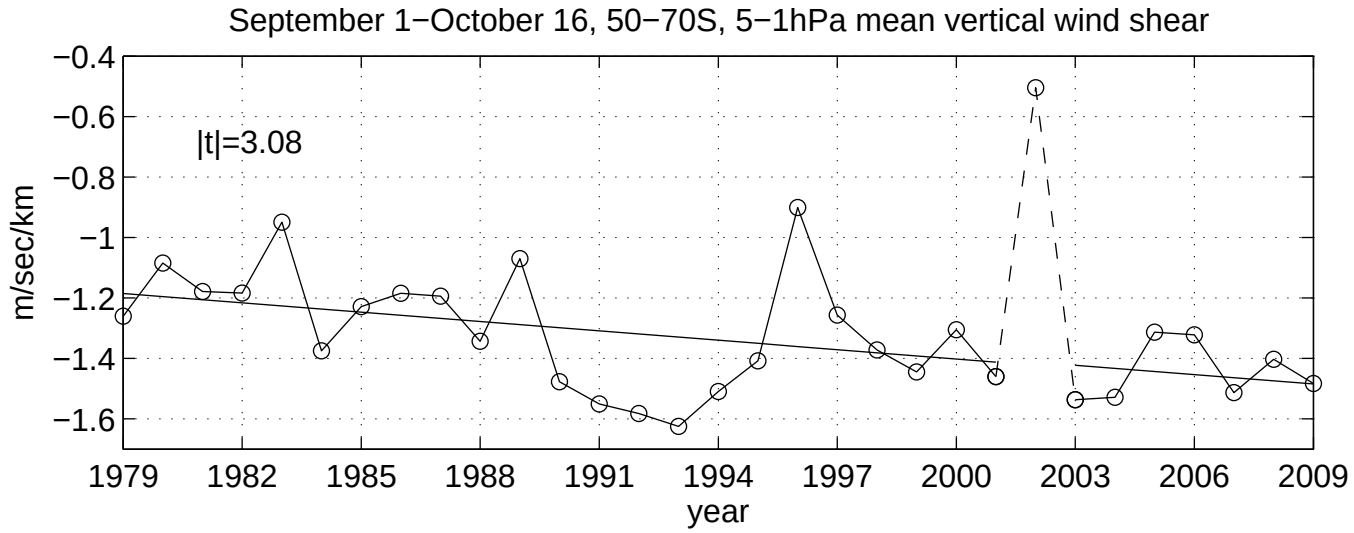

Figure 4: Yearly values of the September 1-October 16 mean vertical shear of the zonal mean wind, averaged over $5-1hPa$, $50-70^oS$ ($msec^{-1}/km$), along with the linear best fit regression. The sudden warming year 2002 is removed from the trend calculation.

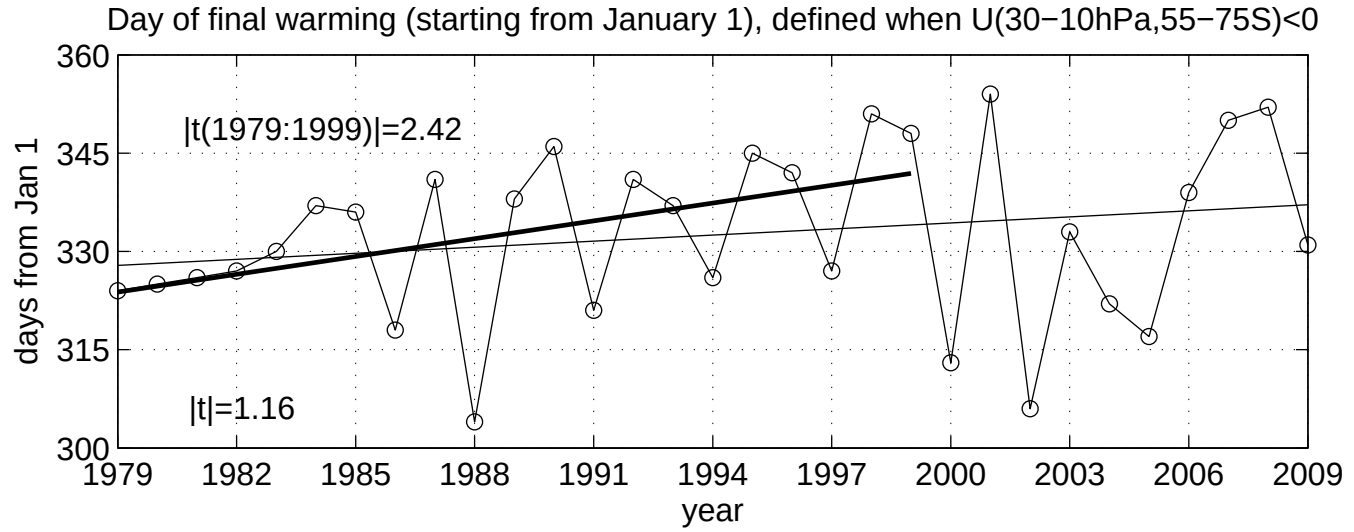

Figure 5: Yearly time series (circled line) with the linear trends and $|t|$ values based on 1979-2009 and 1979-1999 (thin and thick straight lines respectively) of the day on which the zonal mean wind, averaged over $30-10hPa$ $54-75^oS$, first becomes zero, counting from January 1 (excluding the September 2002 sudden warming).

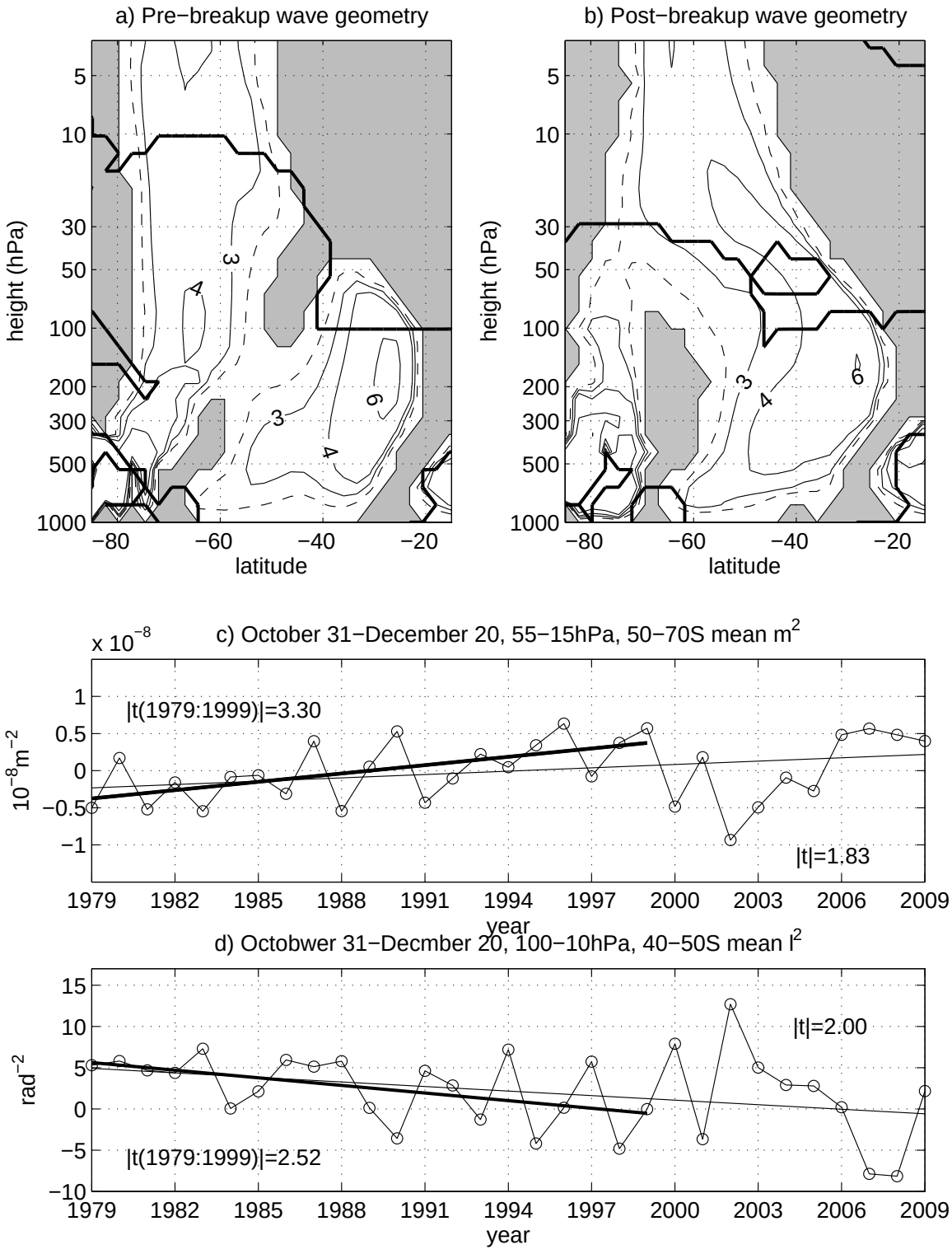

Figure 6: a-b) The 1979-2009 mean vertical and meridional wavenumbers for the 20 days before (a) and after (b) the final warming date, defined by the index of Fig. 5. The contouring and shading in plots a-b are the same as in Fig 3a-c. (c-d) Yearly time series (circled line) with the linear trends based on 1979-2009 and 1979-1999 (thin and thick straight lines respectively) of the October 31-December 20 mean c) vertical wavenumber squared averaged over $55-15hPa$, $50-70^oS$ (units of $10^{-8}m^{-2}$) and d) meridional wavenumbers squared, averaged over $100-10hPa$, $40-50^oS$ (units of rad^{-2}).